


Article

Influence of Spacers and Skid Sizes on Heat Treatment of Large Forgings within an Industrial Electric Furnace

Sajad Mirzaei ^{1,*}, Nima Bohlooli Arkhazloo ¹, Farzad Bazdidi-Tehrani ², Jean-Benoit Morin ³, Abdelhalim Loucif ³ and Mohammad Jahazi ^{1,*} 

¹ Département de Génie Mécanique, École de Technologie Supérieure, Montréal, QC H3C 1K3, Canada
² School of Mechanical Engineering, Iran University of Science and Technology, Tehran 16846-13114, Iran
³ Finkl Steel Inc., Sorel-Tracy, QC J3R 3M8, Canada
* Correspondence: sajad.mirzaei.1@ens.etsmtl.ca (S.M.); mohammad.jahazi@etsmtl.ca (M.J.);
Tel.: +1-(514)-235-5280 (S.M.); Fax: +1-(514)-396-8530 (M.J.)

Abstract: The influence of stacking patterns, through the different spacer and skid sizes, on the transient temperature distribution uniformity of large-size forgings in a 112-m³ electrical heat treatment furnace was investigated by conducting CFD simulations and real-scale experimental validation. A 3D CFD model of the electrical furnace was generated, including a heat-treating chamber, axial flow fans, large size blocks, skids, and spacers. Real-scale temperature measurements on instrumented test blocks during the heat treatment process were carried out to validate the CFD simulations. Results indicated that the CFD model was capable enough to determine the transient temperature evolution of the blocks with a maximum average deviation of about 6.62% compared to the experimental measurements. It was found that significant temperature non-uniformities of up to 379 K on the surfaces of the blocks due to the non-optimum stacking pattern were experienced by the blocks. Such non-uniformities could be reduced between 24% to 32% if well-adapted spacer and skid sizes were used in the stacking configurations. Based on simulation results and experimental validation work, optimum spacer and skid sizes for uniform temperature distribution were proposed for different stacking patterns.



Citation: Mirzaei, S.; Bohlooli Arkhazloo, N.; Bazdidi-Tehrani, F.; Morin, J.-B.; Loucif, A.; Jahazi, M. Influence of Spacers and Skid Sizes on Heat Treatment of Large Forgings within an Industrial Electric Furnace. *Energies* **2023**, *16*, 2936. <https://doi.org/10.3390/en16072936>

Academic Editors: Pino Sabia and Giancarlo Sorrentino

Received: 27 January 2023
Revised: 1 March 2023
Accepted: 21 March 2023
Published: 23 March 2023



Copyright: © 2023 by the authors. Licensee MDPI, Basel, Switzerland. This article is an open access article distributed under the terms and conditions of the Creative Commons Attribution (CC BY) license (<https://creativecommons.org/licenses/by/4.0/>).

Keywords: electrical furnace; computational fluid dynamics; multiple reference frame model; stacking pattern; temperature uniformity; spacer size; skid size

1. Introduction

High temperature industrial furnaces, in which the heat generation is mainly based on fossil fuel combustion or electricity, play a vital role in the iron and steel making industry. Energy saving in such furnaces directly limits the environmental footprint of steel-making industries, which has been reported to be among the top five most energy-intensive industry sectors [1]. Furthermore, such an energy saving could significantly affect the final production cost [2,3]. Heat treatment processes are among the key contributors to energy usage in the iron and steel making industries. A heat treatment process called Quench and Temper (Q&T) is usually employed to obtain desirable properties in large-size high strength steel parts, such as dies or turbine shafts [4]. The mechanical properties of the product, such as resistance, hardness, and toughness, are highly dependent on the cooling cycle and its parameters, such as quenching medium (oil, water, etc.), cooling time, quenching temperature, as well as tempering process parameters, which directly affect the metallurgical transformations of the steels. The tempering step is of crucial importance to the final mechanical properties of the product as major microstructural changes and metallurgical improvements take place during this step [5]. These metallurgical interactions, such as the hardness reduction of brittle quench-hardened steel, improved toughness, and stress relieving, fundamentally depend on the tempering temperature and holding time in the heat treatment furnace [6,7]. It has been reported that non-uniform temperature

distribution may result in non-uniform properties around the products and in some cases scrapping of the part [8,9]. At the present time, most of the existing heat treatment furnaces in the steel industry use natural gas as the heating source, and significant efforts have been devoted to the optimization of the tempering process in such furnaces [10]. However, in recent years, with the implementation of new regulations on the reduction of global carbon dioxide emissions and fossil fuel usage, there has been significant growth in the employment of electrical batch-type furnaces for steel heat treatment processes, but, in contrast to gas-fired furnaces, very little data is available in the case of electrical furnaces, particularly industrial-sized ones. Thus, the accurate prediction and control of the transient temperature distribution and heat transfer to products in electrical furnaces are critical in order to optimize temperature uniformity and fluid flow circulation, similar to what was previously reported by Bohlooli et al. for gas-fired furnaces [11,12]. The optimization process becomes even more complex when, due to production imperatives, multiple loading patterns and stacking configurations must be taken into account as they significantly affect the temperature distributions around the parts [9].

Improving the current practice in the industry, which is mostly based on empirical correlations that could result in significant deviations [5,13], necessitates a comprehensive and systematic quantitative analysis of thermal interactions within the heating chamber. Due to the complexity of the thermal field associated with turbulence and conjugate heat transfer, numerical analysis and simulation tools need to be used [5,7]. This is also because of the fact that the experimental measurements and data acquisition are quite challenging to perform due to the high temperature ranges, size of furnaces and products, limited physical access, and huge instrumentation expenditure.

Recently, computational fluid dynamics (CFD), offering the simultaneous analysis of turbulent fluid flow and conjugate heat transfer, has been employed in several studies on the thermal analysis of industrial furnaces [13–16]. Studies comprising Harish et al. [17] and Zhang et al. [13], or recently published papers such as those by Mayr et al. [18], Tang et al. [19], and Liu et al. [20], employed CFD simulations to investigate the heating procedure in different continuous reheating furnaces (for instance, pusher type furnaces or walking beam furnaces). On the other hand, batch-type heat treatment furnaces used in the tempering process, due to their longer process time (more than 24 h of heating and 48 h of holding for the large size products [8]) require higher computational costs for the complete transient simulations compared to the continuous furnaces. Such a longer process time and problems regarding physical access to the heating chamber also require more attention in the instrumentation for the experimental measurements [16].

Thus, the number of papers available such a context is few and there is little information on the stacking pattern optimization of large-size blocks within real-scale heat treatment furnaces. The existing studies have been narrowed to investigations in the laboratory to semi-industrial medium-scale furnaces [21–23], or only to furnace medium analysis rather than simultaneous analysis of thermal interactions between the chamber medium and product [24,25]. For instance, using CFD simulations, Filipponi et al. [26] investigated the effect of the door opening on the temperature distribution of unloaded batch-type gas-fired furnaces. The objectives of the reviewed literature were mainly focused on the temperature distribution of products in the conventional process rather than the subsequent optimization of the process. Among the rarely found studies on the optimization side, Palacio et al. [2] used CFD simulations to present a detailed investigation of the influence of fans' rotational speed on the temperature uniformity of the product within an electrical convective heat treatment furnace. Díaz-Ovalle et al. [27] reported that the baffle plate geometry in an electrical convective furnace could have an important influence on the temperature uniformity of the furnace and the preheating time of the furnace. Using a 3D numerical model, Tan et al. [28] simulated the heat transfer during annealing in a vertical furnace to recommend design changes that would improve thermal uniformity across the stacked wafers. In the simulation, it was found that the heat loss at the process door was greater than the heat loss at the top header. Their suggestions could lead to a reduction in

heat loss and an improvement in the thermal uniformity of stacked wafers. Food industry researchers Amanlou et al. [29] developed numerical CFD models of a heating oven (cabinet dryer). In their work, they addressed the non-uniformity in the moisture content of the end product after the heat treatment. The CFD model simulated the airflow and temperature distribution inside the drying chamber, which is very similar to the challenges faced in steel industry furnaces. A similar study was carried out on a forced convection oven to investigate the isothermal airflow for a quick baking process by Ismail et al. [30]. The results of their study demonstrated the importance of impeller placement in the performance of the oven. Using the commercial CFD software FLUENT, Fu et al. [31] developed an innovative approach to simulate the heating process of a superalloy workpiece in a laboratory-scale electric furnace. The model mainly focused on the heat generation rate of the energy source developed using FLUENT user-defined function (UDF); a proportional integral derivative (PID) method was proposed to regulate furnace temperature according to the thermal scheme. Arkhazloo et al. [9], investigating the thermal interactions inside an industrial gas-fired furnace, reported the significant effect of stacking patterns (such as their relative locations and distances) on the uniformity of the tempering process. Such influence on the temperature uniformity of the product was also mentioned by Wang and Shang [15] and Macchion et al. [32] in their numerical studies of small-scale steel parts' heat treatment within a high pressure gas quenching chamber. According to Macchion et al. [32], the temperature uniformity of the product was significantly affected by the position of parts within the furnace. Korad et al. [33] used steady-state CFD simulations to study the aluminum billet heat treatment inside a homogenization furnace. Their results indicated that the different billets experienced different temperature distributions as a result of the stacking pattern and their relative locations within the heating chamber.

However, up to now, little information has been available on the influence of stacking pattern parameters such as spacers and skid sizes on the temperature uniformity of large size steel parts within an industrial electrical heat treatment furnace. Therefore, the present study investigated the influence of stacking pattern parameters on the uniformity of large size products' heat treatment process and their corresponding transient heating rates within an industrial electrical heat treatment furnace. Stacking pattern parameters and their relative positions were discussed using unsteady CFD simulations of the process. The three-dimensional (3D) CFD model of the electrical batch-type heat treatment furnace encompassed all the details of the 112 m³ furnace, including axial fans, large-size forged blocks, and skids. Details of the numerical simulations, including initial and boundary conditions, were specified using experimental measurements, and the corresponding data are provided. Numerical predictions were validated using temperature measurements around instrumented 29-metric-tons large-size forged blocks during the heat treatment process. Results were analyzed and interpreted in terms of the conjugate heat transfer modes and their corresponding interactions related to the temperature distribution of large-size blocks due to the stacking pattern alterations.

2. Furnace Description

The present research was carried out on an industrial electrical heat treatment furnace located at Finkl Steel, Sorel, QC, Canada [34]. This batch-type car bottom furnace has two series of heating elements located on the two side walls of the heating chamber. Three axial fans are mounted on top of the furnace chamber to allow the flow of the hot air inside the chamber and around the blocks. These three fans, namely front, center, and back, have a constant rotational speed of 1750 rpm. The central fan rotates clockwise, while the other two fans have counterclockwise rotational directions, which are dependent on the fans' blades angle. In these high temperature fans, air flows through the blades and parallel to the shaft on which the fans are mounted. A vertical distance of 1.27 m is between the axial fans and the heating elements. Figure 1 shows the electric furnace and its corresponding drawings, including the dimensions of the heating chamber and its details (such as skids, axial fans, and typical loading zone). Details of the fans and electrical heating elements, highlighted

by red circles, can be seen in this figure. The internal dimensions of the heating chamber of the furnace are 3.43 m, 4.11 m, and 8.02 m in the x, y, and z directions, respectively. Five steel skids with a cross-section of $0.27 \text{ m} \times 0.27 \text{ m}$ and a length of 3.05 m are placed to locate the large forged blocks on the car bottom furnace. Fans circulate fluid flow to heat the products, and the furnace has no exhaust. The furnace walls are covered using refractory ceramic fibers with a thickness of 0.254 m and a thermal conductivity of $0.16 \text{ W}/(\text{m}\cdot\text{K})$ at $538 \text{ }^\circ\text{C}$ (corresponding to the tempering temperature).

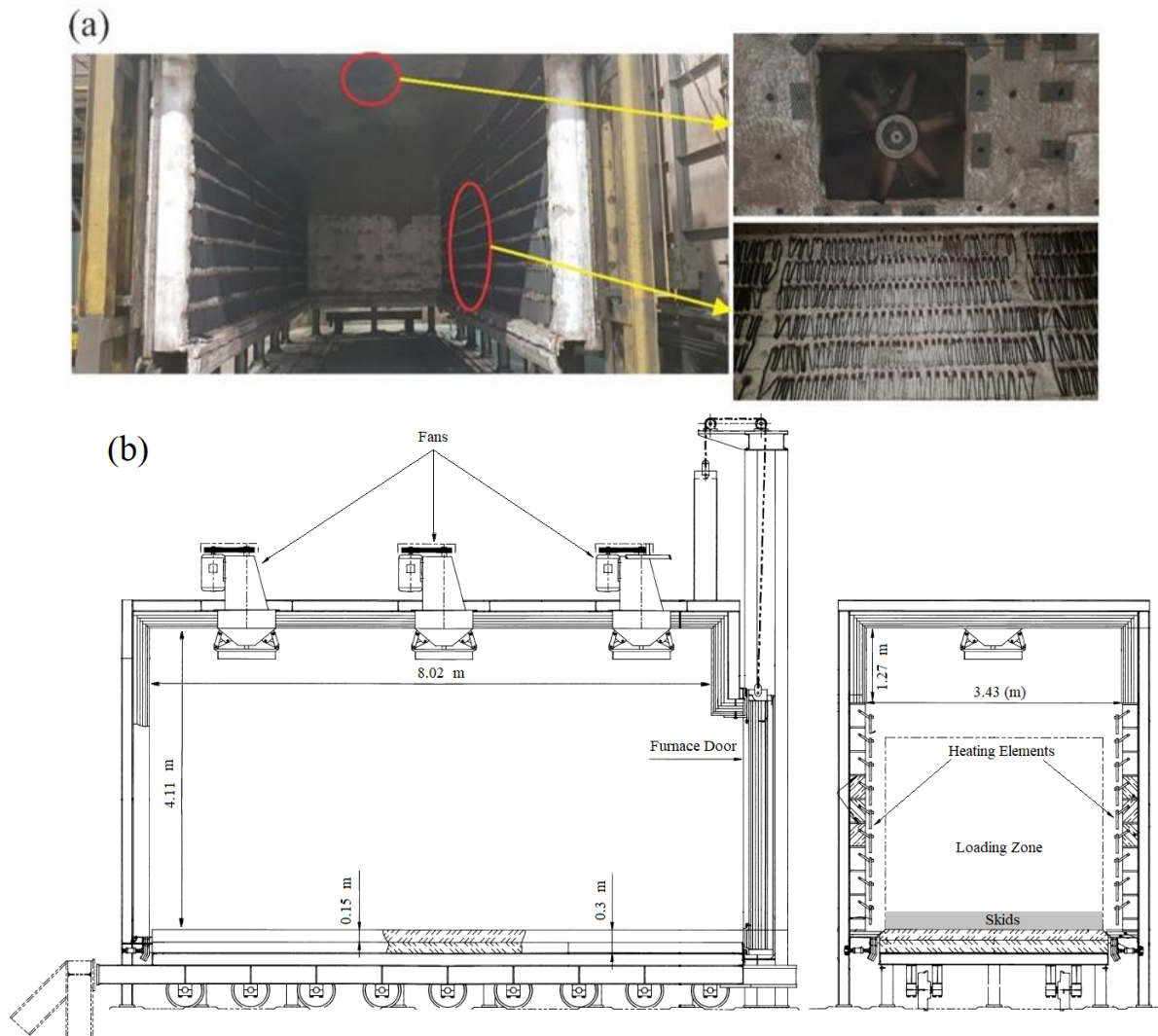


Figure 1. (a) Car bottom electrical furnace and (b) its corresponding drawings and dimensions [34].

3. Stacking Patterns

Two main configurations (configs) of stacking with different forging sizes were considered for the analysis:

- **Config-1:** This stacking pattern consisted of two large sizes rectangular parallelepiped-shaped forgings with the dimensions of $1.34 \times 0.66 \times 4.25 \text{ m}^3$ and $1.27 \times 0.63 \times 4.6 \text{ m}^3$, named hereafter as upper and lower blocks, located on the car bottom of the furnace. Config-1 provides an insight into the heat treatment of high thickness forgings in this furnace.
- **Config-2:** Three stacked blocks with the corresponding dimensions of $1.2 \times 0.25 \times 4.36 \text{ m}^3$, $1.2 \times 0.25 \times 3.88 \text{ m}^3$, and $1.2 \times 0.25 \times 4.2 \text{ m}^3$, called upper, middle, and lower blocks, respectively, were used to evaluate the stacking pattern effect on the heat treatment of blocks.

These two configs were subjected to the usage of several spacer and skid sizes to evaluate their effect on the temperature uniformity of the products. The following secondary level naming format was used to refer to each case under investigation:

- -S5, -S12, -S17, and -S25: Referring to the cubic spacer sizes of $0.05 \times 0.05 \times 0.05 \text{ m}^3$, $0.12 \times 0.12 \times 0.12 \text{ m}^3$, $0.17 \times 0.17 \times 0.17 \text{ m}^3$, and $0.25 \times 0.25 \times 0.25 \text{ m}^3$, respectively.
- -DSK: To identify the effect of double-size skids on the analysis.
- Figure 2 represents the discussed blocks in the two defined configs located on the car bottom of the electrical furnace with -S5 spacers.

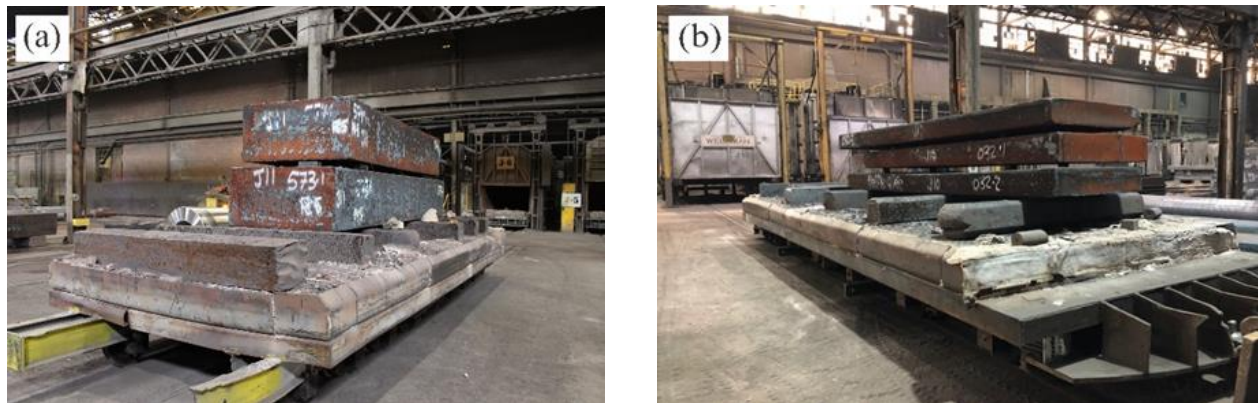


Figure 2. Industrial scale stacking patterns: (a) Config-1-S5 and (b) Config-2-S5.

4. Experimental Measurements

Temperature measurements were conducted using five pre-calibrated [35] K-type thermocouples (TC) with a stainless steel sheath. These TCs were positioned in different locations of the forgings' surfaces in Config-1. Figure 3 depicts the industrial scale experimental setup and its corresponding schematic view. Thus, “L” and “l” are the lengths of the lower block and upper block, respectively, “H” is the height of the lower block, and “w” is the weight of the upper block. Details regarding the methods developed for reliable data acquisition were published in a recent article by Arkhazloo et al. [11]. Figure 4 displays the transient history of the electrical energy usage profile at 600 V and 60 Hz power by the loaded furnace during the heat treatment process.

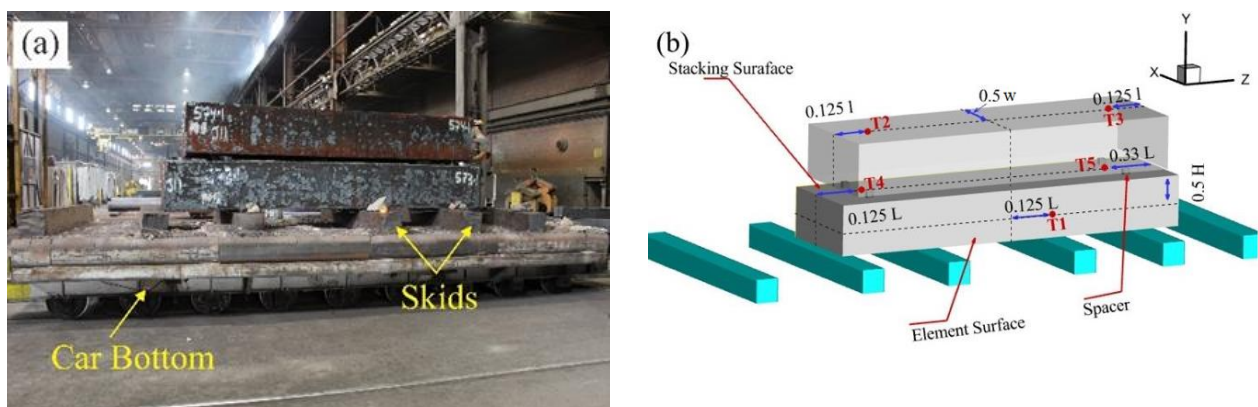


Figure 3. Experimental setup details including (a) real-scale experimental configuration and (b) a schematic view of five thermocouples' locations (T1–T5).

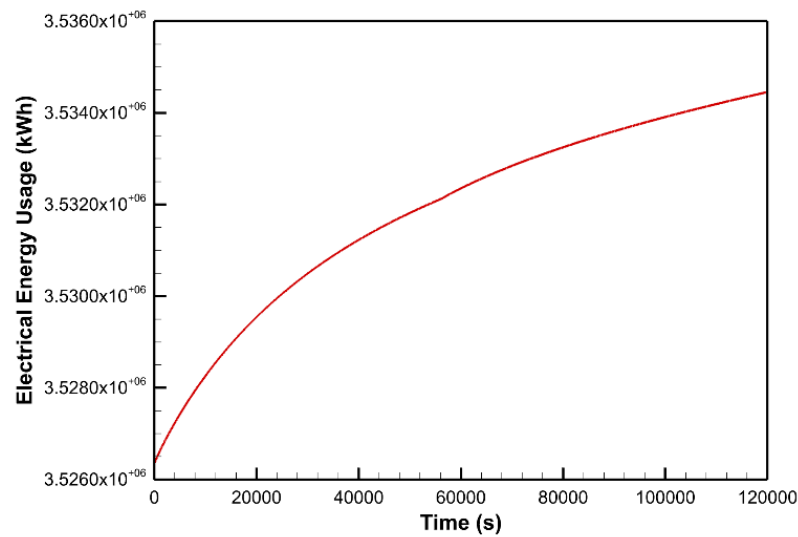


Figure 4. Transient history of electrical energy usage profile versus time, at 600 V and 60 Hz power consumed by the heating elements in the furnace.

5. Computational Details

5.1. Governing Equations

A transient CFD simulation with a multiple reference frame (MRF) model was used to solve the Reynolds-averaged Navier-Stokes equations [36]. Generally, MRF transforms the fluid equation of motion to a rotating frame so that the steady-state solutions for the rotating frame are possible. This model can be applied to a steadily rotating part of a domain with constant rotational speeds. The method was reported to be reliable, especially in cases where the flow outside of the rotating frame is of interest [36]. In the current study, the computational domain was divided into three rotating references (three fans with a constant rotational speed of 1750 rpm) and one stationary frame (furnace chamber outside the region of the fans, including blocks). The governing equation of fluid flow for fan zones in absolute velocity formulation is as follows:

$$\frac{\partial \rho}{\partial t} + \nabla \cdot (\rho \vec{v}_r) = 0 \quad (1)$$

$$\frac{\partial}{\partial t} (\rho \vec{v}_r) + \nabla \cdot (\rho \vec{v}_r \vec{v}) + \rho (\vec{\omega} \times \vec{v}) = -\nabla p + \nabla \cdot \bar{\tau} + F \quad (2)$$

$$\frac{\partial}{\partial t} (\rho E) + \nabla \cdot (\rho \vec{v}_r H + p \vec{u}_r) = \nabla \cdot (k \nabla T + \bar{\tau} \cdot \vec{v}_r) + S_h \quad (3)$$

where, \vec{v}_r and \vec{u}_r are defined as a function of \vec{r} (position vector of a point from the origin of the rotating frame), as follows:

$$\vec{v}_r = \vec{v} - \vec{u}_r, \quad \vec{u}_r = \vec{\omega} \times \vec{r} \quad (4)$$

The rotational speed for the furnace chamber (except the rotating fans at 1750 rpm) is equal to zero ($\omega = 0$), which results in stationary forms of equations. It should be mentioned that a local reference frame transformation is considered for the flow variables at the interface between the zones to have consistent predictions of fluxes. However, scalars, including temperature and pressure, are passed without changes.

The turbulence induced by the fan rotations was simulated using the Realizable k- ϵ model. It has been reported that this model has shown good agreement with experimental observations in heat treatment processes [16].

Finally, the surface-to-surface (S2S) model [36] was employed to compute the radiation heat transfer to the blocks from the furnace medium, skids, and adjacent blocks within the heat treatment chamber. In this model, the radiative heat transfer equation is simplified by considering only the surface-to-surface radiation, as follows: (i.e., ignoring the medium's absorption, emission, or scattering effect on the radiation heat transfer) [36].

$$q_{out,k} = \varepsilon_k \sigma T_k^4 + \rho_k \sum_{j=1}^N F_{kj} q_{in,k} \quad (5)$$

where, $q_{out,k}$ is the energy flux leaving the surface k and $q_{in,k}$ is the energy flux incident on the surface from the surroundings. ε_k , ρ_k , and T_k are the emissivity coefficient, reflection coefficient, and temperature of surface k , respectively. F_{kj} is defined as the view factor between surface k and surface j , and σ is the Stefan-Boltzmann constant.

5.2. Model Description

Simulations were carried out using ANSYS FLUENT 2021 R2 software, based on the finite volume method applying the unsteady SIMPLE algorithm [37] to non-uniform hexahedral computational grids. A schematic view of the computational domain, including the boundary conditions and details of the heating chamber corresponding to the experimental measurements, is also presented in Figure 5. Three sets of meshes including 758,000, 3,155,000, and 10,576,000 cells, named coarse, medium, and fine mesh, respectively, were created to verify the independence of results from mesh size. It was found that the medium mesh performed reasonable predictions compared to the fine mesh, and the prediction differences were negligible. Therefore, the medium case with 3,155,000 cells was employed for the rest of the simulations. An average heat loss of 594 W/m^2 was applied to the furnace walls. This value was calculated in accordance with the approach proposed by Hadala et al. [38]. Standard wall functions were applied to the no-slip condition walls, including furnace walls and forgings surfaces. The steel blocks' surface emissivity (ε) was set to 0.8, while an emissivity of 0.75 was considered for the furnace refractories. The effect of heating elements was considered using transient heat flux through the side walls. Transient temperature-dependent thermophysical properties of the materials were calculated using the JMatPro 11 software [39]. The steel under investigation was a high strength medium carbon steel-modified P20.

It should be mentioned that during the transient calculations, each time step continued up to a convergence of 10^{-5} , 10^{-6} , and 10^{-9} for the continuity, energy, and radiation equations, respectively.

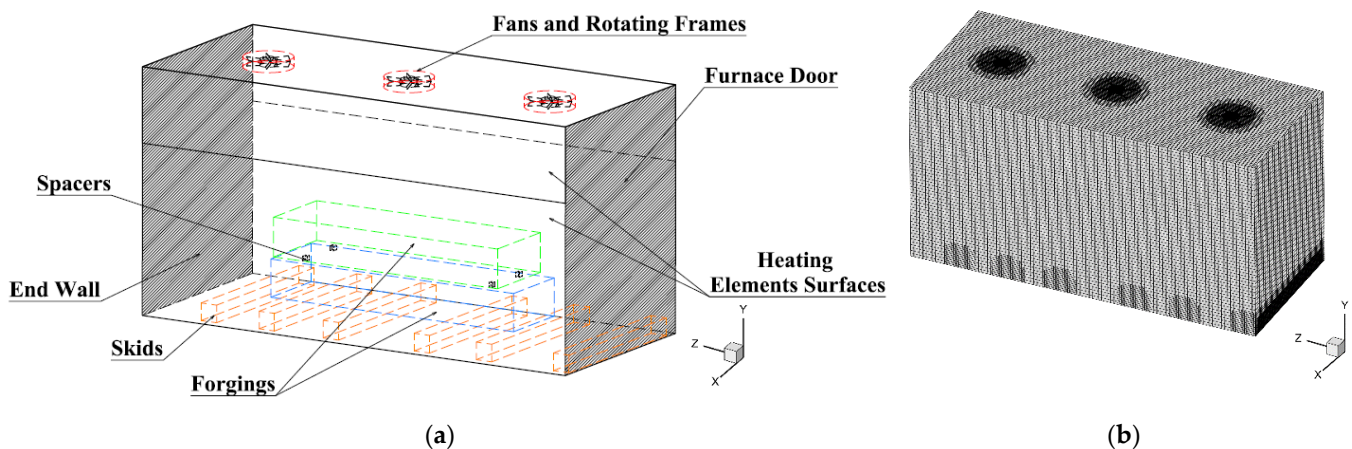


Figure 5. (a) The computational domain including solid zones, walls, heating elements surfaces, fans, and rotating frames and (b) computational grids for the CFD simulations.

6. Results and Discussion

6.1. Validation

The measured transient temperatures of the forged blocks' surfaces at different TCs locations and the corresponding CFD model predictions are represented in Figure 6. It can be seen that there is a noticeable difference between the transient temperature histories of different TCs during the heat treatment process, which will be discussed in detail in the following subsections. The CFD predictions showed reliable consistency as compared to the measurements. The results of the CFD model predictions at the TCs locations displayed a very good agreement with a maximum average of about 6.62% deviation compared to the experimental measurements. Owing to the consistency between the predictions and measurements, it can be concluded that the CFD model with the MRF, which requires a lower computational cost and inherits a better converging trend compared to the dynamic mesh modeling, was reliable in the context of the present study. Therefore, this model was employed to evaluate the influence of different stacking patterns and spacer sizes on the heating history of the large-size blocks in the application under investigation.

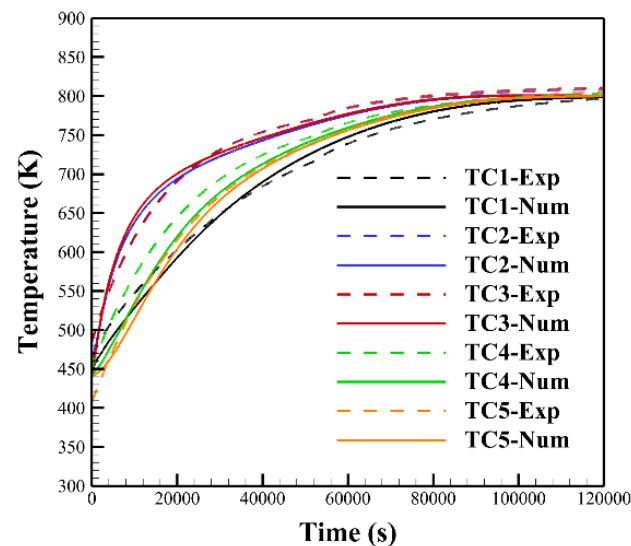


Figure 6. Validation of CFD simulations with the MRF model.

6.2. Config-1 Analysis

The transient evolution of maximum temperature non-uniformities of large-size blocks during the heat treatment process in Config-1 is shown in Figure 7. The maximum temperature non-uniformity (ΔT) was defined as an instantaneous temperature difference between two points on the surfaces of the blocks, which experienced the maximum and the minimum temperatures, respectively. It can be seen that both blocks experienced significant non-uniformities during the heat treatment process. Such non-uniformity was also reported for gas-fired furnaces [9,16]. This temperature non-uniformity is not usually considered in metallurgical investigations of the heat treatment process, where the main attention is concentrated on the temperature gradient between the center and surface of the block. It can be observed that the curves had an increasing trend up to 0.1 of the total heat treatment time ($t/t_T \sim 0.1$) when the maximum non-uniformities of 195 K and 200 K were produced around the lower block and upper block, respectively. Then, the non-uniformities were reduced to a certain level at the end of the process, at which the furnace and block were held at the isothermal tempering temperature of 800 K. However, it should be noted that such non-uniformities were experienced even after 6 h of tempering (by about 176 K for the lower block) and could significantly affect the mechanical properties of the final product from one end of the product to another.

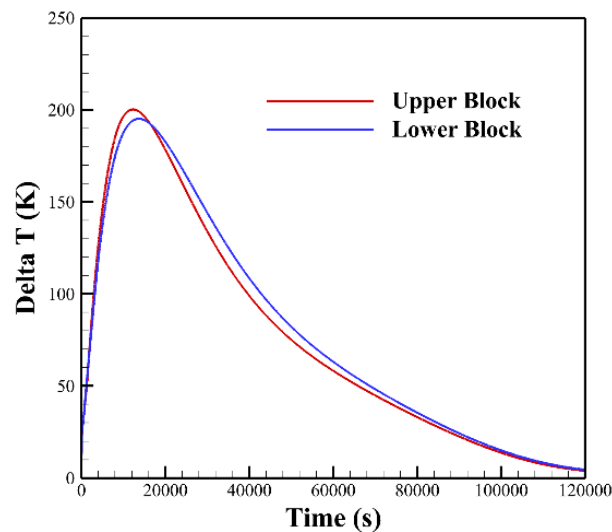


Figure 7. Transient temperature non-uniformities experienced by different blocks of Config-1-S0 during the heat treatment process.

To determine the effect of spacer usage on the temperature distribution of blocks during the process, contours of the temperature distribution at the central cross-section of the blocks in Config-1-S0 and Config-1-S5 at $t/t_T = 0.1$, when the maximum non-uniformities were identified, are depicted in Figure 8. From Figure 8a, for Config-1-S0, both blocks experienced an uncommon temperature gradient from different surfaces to the center of the block. Ideally, it is expected that the blocks have a uniform increasing temperature from the center to the surface of the block with approximately the same temperature at equal depths. However, results not only showed that the different surfaces of the blocks followed different temperature patterns, but that the minimum temperature was also not located at the center of the block, but shifted toward the blocks' stacking surfaces. This was more evident in the upper block, whose minimum temperature was located on its lower surface (stacking surface). It could be seen that in this block, a reducing temperature gradient occurred from the upper left and upper right corners toward the lower surface. Furthermore, a similar trend was found for the lower block, the minimum temperature of which was identified at the upper surface. Such an irregular temperature gradient for the large-size blocks was also reported by Arkhazloo et al. [9,16] for the heat treatment within a gas-fired furnace. According to [16], although the unloaded gas-fired furnace was uniform during the conventional uniformity test, blocks showed significant temperature non-uniformities after loading and during the heat treatment process of products. The reason was due to the size of the products, which extremely affected the furnace flow field, including vortical structures and thermal boundary layers. Given the temperature uniformity of the unloaded furnace in the present study, it can be said that the similar effect of large-size products on the fluid flow circulation within the electric furnace is the reason behind the identified temperature non-uniformities.

The results indicate that using -S5 spacers contributes to shifting the coldest point toward the blocks' center and reduces the sharp temperature gradient at this cross-section compared with Config-1-S0. In addition, the use of spacers appears to result in higher temperatures at the block center (shrinkage of contour's minimum level) in Config-1-S5 compared to Config-1-S0. Therefore, it can be said that not only could the spacers contribute to the uniformity of the temperature distribution during the heat treatment process, but they also result in higher heating rates compared to the conventional stacking method without spacers.

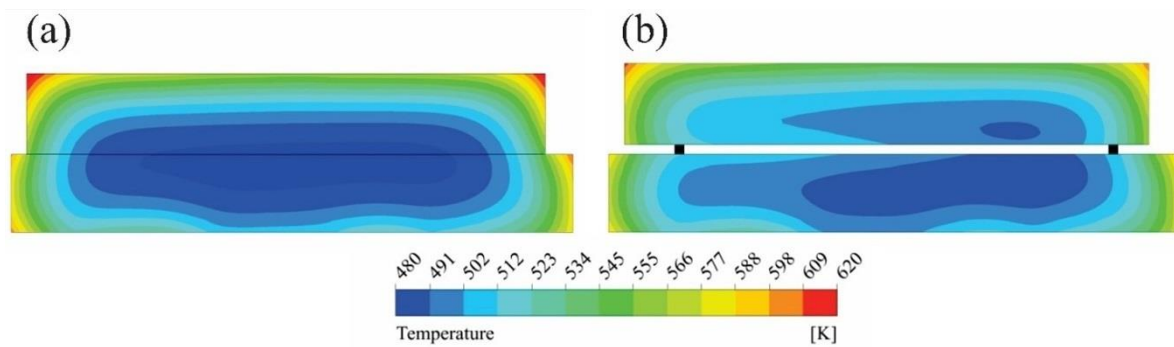


Figure 8. Contours of temperature distribution at the central cross-section of blocks at $t/t_T = 0.1$ (a) Config-1-S0 and (b) Config-1-S5.

The influence of the spacer size on temperature uniformity was also investigated. The results are presented in Figure 9, where the transient history of block non-uniformities in Config-1 is compared for different spacer sizes. It can be seen that there is a significant reduction in the maximum temperature non-uniformities of blocks (peak of the non-uniformity curves) as a result of spacer usage. The data presented in Figure 9 also shows that even small spacers (-S5) could considerably reduce the maximum non-uniformities by about 19% and 23% for the upper and lower blocks, respectively. However, it is interesting to note that larger spacer sizes would not always lead to a reduction in the maximum non-uniformities because they could also act as heat sinks. Hence, depending on the size and mass of the spacers, they can lead to a local temperature non-uniformity. For instance, the maximum non-uniformity of the lower block (Figure 9a) for the -S12 and -S25 cases are higher than those of -S5 and -S17, respectively. Therefore, although an increase in the spacer size from -S5 to -S17 resulted in a reduction of temperature non-uniformity by about 11%, the increase in the spacer size from -S5 to -S12 increased the maximum temperature non-uniformity of the products. In this stacking pattern, it could be said that the -S17 showed the optimum efficiency characterized by the minimum temperature non-uniformities around the blocks.

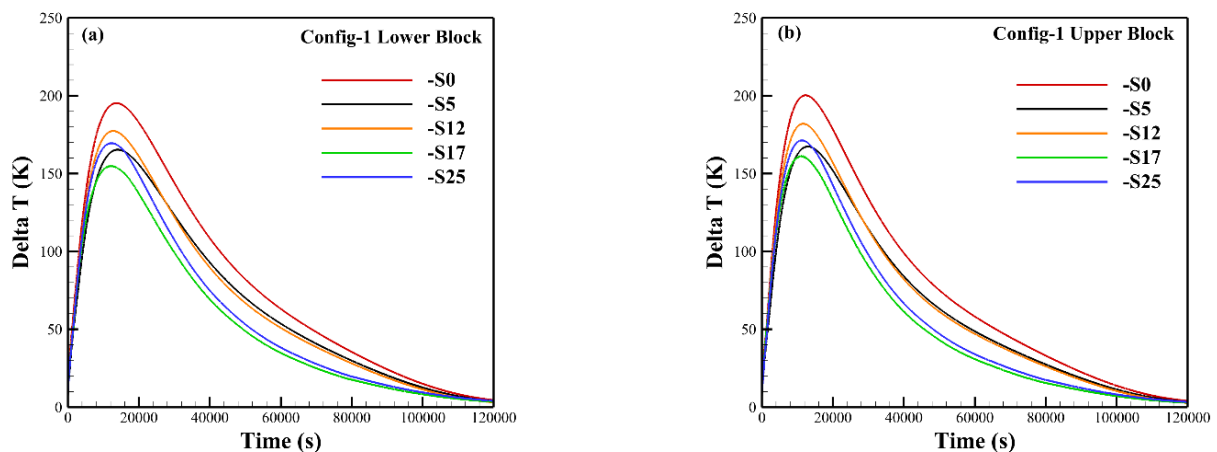


Figure 9. Effect of spacer size on temperature non-uniformities of products in Config-1: (a) lower block and (b) upper block.

In addition, the area under each curve in Figure 9 represents the total non-uniformity that a block experienced during the heat treatment process. In other words, the differences between the area under the curves determine the difference between the total transient temperature non-uniformities experienced by the blocks. Table 1 presents the total temperature non-uniformity reductions due to the usage of different spacer sizes compared to Config-1-S0. Results in Figure 9 and Table 1 show that the area under cases with spacers were clearly contracted compared to Config-1-S0. It should be noted that these contractions were not only on the peak areas of the curves, but also on the secondary descending part

of the curves when the blocks were at higher temperatures (close to the target tempering temperatures). Therefore, the positive effect of spacers is not just about the early stage of the process, but is rather evident throughout the entire process. Analysis of the obtained results indicated that the maximum shrinkage belonged to the -S17, with about a 23% and a 26% reduction compared with -S0 for the upper and lower blocks, respectively. It can be seen that the -S17 with both reduction on the peak and tail of the curve could present more effective performance compared to the other spacers.

Table 1. Total temperature non-uniformity reduction of blocks with different spacer sizes in Config-1 compared to Config-1-S0.

Products	-S5	-S12	-S17	-S25
Lower Block	16%	12%	26%	22%
Upper Block	12%	9%	23%	19%
Average Effectiveness	14%	10.5%	24.5%	20.5

The positive effect of spacers could be discussed by considering different heat transfer modes during the process. Specifically, the presence of the spacers contributes to better fluid flow circulation within the heating chamber and around the blocks. This circulation around the block and specifically around the stacking surfaces results in the accession of convection heat transfer at those specific surfaces. Furthermore, the space between the blocks enhances the absorbed radiation heat from the furnace chamber by those surfaces due to scaling up on the radiation shape factor. Given the temperature ranges, it could be said that the convection heat transfer contribution to the reduction of temperature non-uniformity is mostly related to the peak reduction at the early stage of the process. Because at the early stage of the process both furnace atmosphere and blocks are at lower temperatures, the effect of radiation heat transfer is minor. On the other hand, it can be said that the positive contribution of spacers on the accession of radiation heat transfer is correlated to the secondary part of the curves, in which the area under the tails of the graphs were contracted. Therefore, the superposition of the introduced convection and radiation heat fluxes to the stacking surfaces using spacers results in a reduction of identified temperature non-uniformities compared to those of the conventional stacking pattern (Config-1-S0).

6.3. Config-2 Analysis

The temperature distribution contours of the central cross-section of the three blocks in Config-2-S0 and Config-2-S5 are depicted in Figure 10. The temperature distribution non-uniformities around the blocks are more significant for Config-2-S0, as compared with Config-1-S0, where the three blocks were loaded on the furnace. Contours reveal that the middle block faced an adverse tempering situation in which the block surfaces experienced lower temperatures than the center of the block. Considering the fact that the block's surface areas (upper and lower surfaces) were exposed to a higher cooling rate in the previous step (quenching in water), such an adverse situation could considerably change the metallurgical transformation during the tempering, which should be prudently taken into consideration since this situation is not in accordance with what is expected from the metallurgical point of view for the design of the optimum heat treatment process. A similar trend was also found for the lower and upper blocks, where the minimum temperatures were close to the stacking surfaces, and significant temperature differences were predicted around the blocks. However, it can be seen that the use of spacers in Config-2-S5 resulted in better temperature distribution, and the very low temperature area (blue contours) in the middle block was contracted in Config-2-S5 (Figure 10b). Although the temperature uniformity in Config-2-S5 is not ideal, the minimum temperature, in this case, was shifted toward the center of the block, which is desirable for heat treatment accuracy.

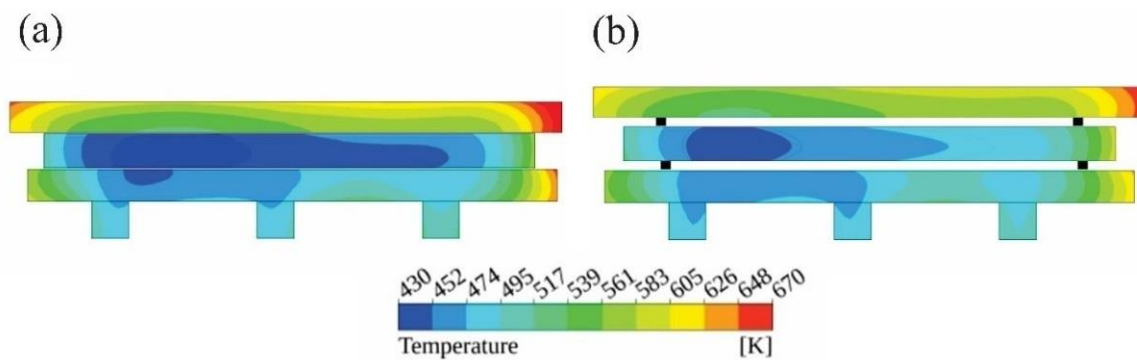


Figure 10. Temperature distribution at the central cross-section of (a) Config-2-S0 and (b) Config-2-S5.

In the case of Config-2-S0, the blocks were located near the furnace's door. Due to this, the minimum temperatures were shifted toward the left side (furnace door), where the door blocked the fluid flow of the furnace. In addition, the effect of skids on the temperature distribution of the lower block can be clearly identified in this figure. The coexistence of the low temperature areas in this block and skids illustrates the effect of skids on the discussed temperature distribution map. This effect can be evidently recognized for both cases in Figure 10. Therefore, in this configuration, the stacking of blocks not only affected the blocks' temperature distribution, but their corresponding orientations with respect to the heating chamber details (i.e., door and skids) also affected the heating thermography.

Another significant fact that should be considered in the results presented in Figure 10a is that the upper block had higher temperatures (i.e., heating rates) compared with the lower and central blocks. This is in contrast to what is expected in an optimum heat treatment process in which uniform and equal heating rates are required for all the blocks in one batch of forgings. Therefore, not only did each block in Config-2-S0 have irregular and significant temperature non-uniformities, but the blocks had completely different heating histories. Such a situation could lead to the rejection of a block in this stacking setup after post-heat treatment inspections. On the other hand, it can be seen that the -S5 spacers in Figure 10b could help in this matter by reducing the temperature difference between the blocks. Nonetheless, because the existing non-uniformities could impact the blocks' final mechanical properties, further evaluation of the spacer and skid sizes should be conducted.

The transient evolution of temperature non-uniformity curves of three blocks for Config 2-S0 are shown in Figure 11. Similar trends to those for the large blocks in the Config-1-S0 are observed. However, a comparison of the maximum non-uniformities of blocks in both cases displayed that the blocks in Config-2-S0 experienced higher temperature non-uniformities. The data analysis in Figure 11 shows that the upper, center, and lower blocks had maximum temperature non-uniformities of 299 K, 379 K, and 337 K, respectively. In other words, although the blocks in Config-2-S0 had smaller dimensions compared to the blocks in Config-1-S0, they experienced more temperature non-uniformities from one end to the other. Such a level of temperature non-uniformity could be related to the loading cycle (i.e., three loads vs. two loads) and also to the orientation of blocks with respect to the furnace details within the heating chamber.

The comparative curves of temperature non-uniformities as a result of five different spacer sizes used in Config-2 are illustrated in Figure 12. The corresponding total temperature non-uniformity reduction values compared to Config-2-S0 are presented in Table 2. The results of Figure 12 prove the positive effect of spacers on the reduction of temperature non-uniformity peaks in Config-2. The maximum temperature non-uniformities as a result of the -S5 spacer usage were reduced from 299 K, 379 K, and 337 K for the upper, middle, and lower blocks (in the -S0 setup) to 205 K, 237 K, and 246 K, respectively. It can be seen that, similar to Figure 9, -S12 and -S25 had lower effectiveness compared to -S5 and -S17, respectively. Furthermore, -S17 displayed the best performance among all the other spacers, with an average temperature non-uniformity reduction of 34% compared to Config-2-S0

(see Table 2). This is in accordance with the good performance of -S17 for the first stacking setup in Config-1. Thus, it can be said that -S17 is the optimum spacer size among the sizes studied for tempering in the present investigation.

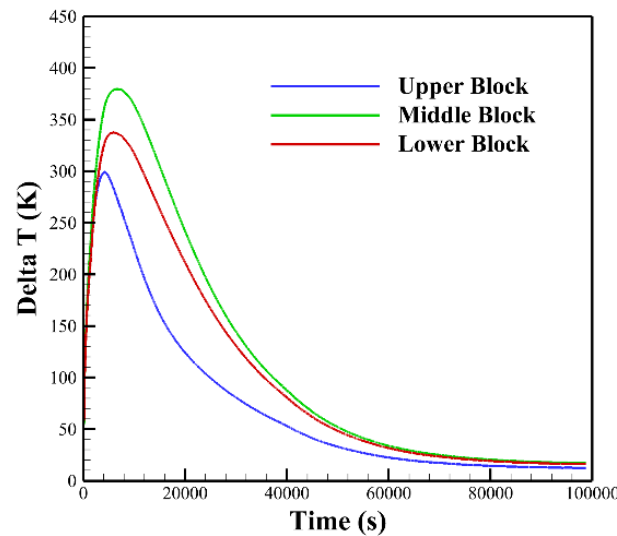


Figure 11. Transient histories of blocks' temperature non-uniformities in Config-2-S0.

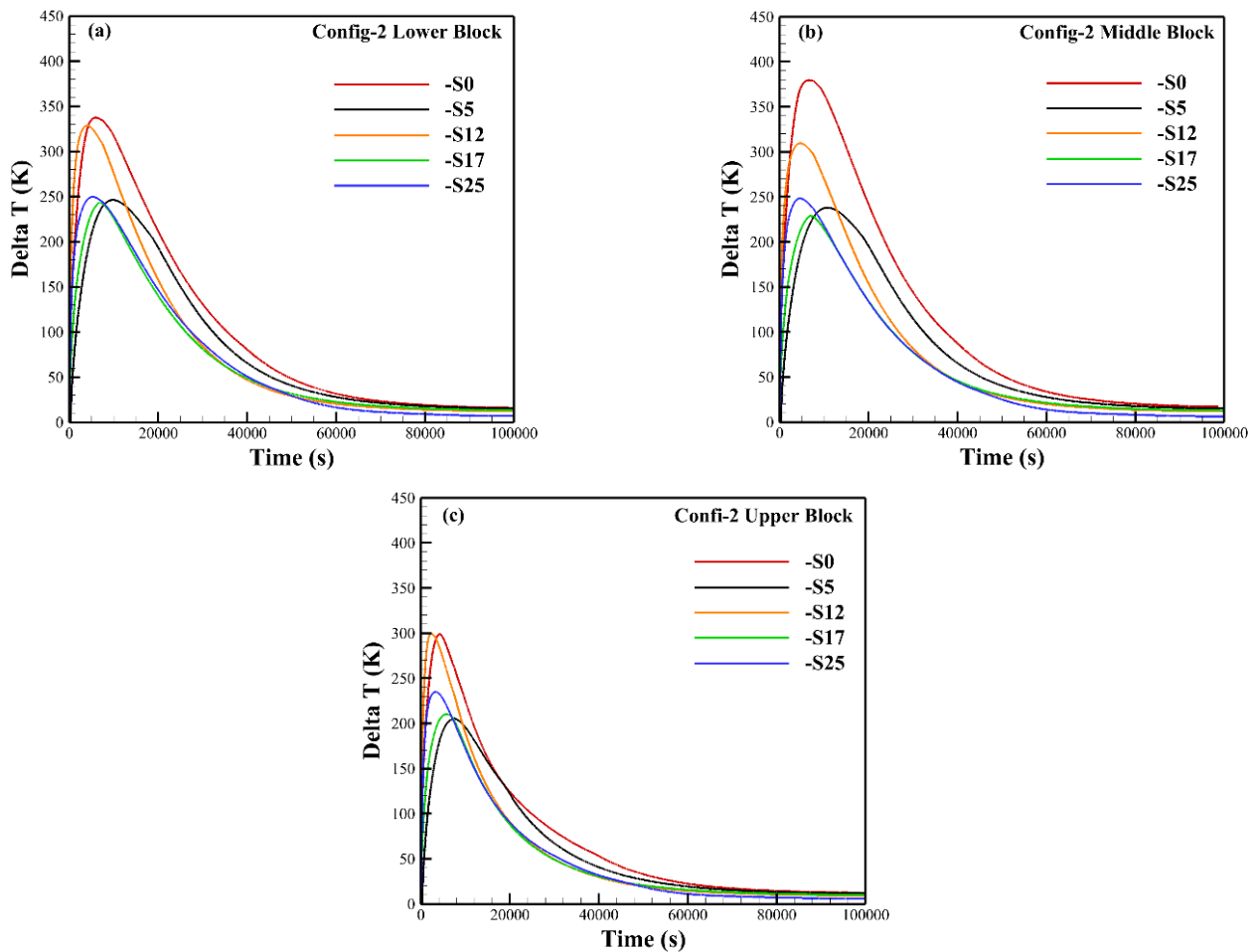


Figure 12. Effect of spacer size on temperature non-uniformities of products in Config-2: (a) lower block, (b) middle block, and (c) upper block.

Table 2. Total temperature non-uniformity reduction of blocks with different spacer sizes in Config-2 compared to Config-2-S0.

Products	-S5	-S12	-S17	-S25
Lower Block	21%	17%	32%	28%
Middle Block	29%	27%	40%	35%
Upper Block	19%	17%	30%	26%
Average Effectiveness	23%	20.3%	34%	29.6%

Furthermore, a comparison of the predictions presented in Figures 11 and 12a,b indicates that although the middle block in Config-2-S0 experienced the maximum non-uniformities, the usage of spacers imposed a situation in which the middle block experienced significantly lower temperature non-uniformities. It can be seen that in the spacer-imposed setups, the lower and middle blocks experienced fairly similar non-uniformities, resulting in a similar heat treatment for the batch of forgings in the furnace.

6.4. Effect of the Double-Size Skid on the Heat Treatment Process

The effect of skid size on the temperature uniformity of blocks during the heat treatment process is illustrated in Figure 13. Figure 13a,b indicate that the use of a double-size skid in the heat treatment process of Config-1 led to a significant reduction of the identified maximum temperature non-uniformity (peak of the curves) and the total non-uniformities (areas under the curves) of both the lower and upper blocks. Analysis of the corresponding data reported in Table 3 shows that the double-size skid resulted in a 5% reduction for -S17 and an average of 14% reduction for the -S5 setups in Config-1. It can be said that the double-size skid contributes to better temperature uniformity by reducing the distance between the fans and the forgings. The effectiveness of such alteration is more significant for the -S5. Therefore, considering the practical difficulties of using -S17 in the production routines, the Config-1-S5-DSK could be effectively used for the heat treatment of large-size products.

Table 3. Effect of the double-size skid on temperature non-uniformity reduction of blocks in Config-1 compared to Config-1-S0.

Products	-S5	-S5-DSK	-S17	-S17-DSK
Lower Block	16%	29%	26%	31%
Upper Block	12%	27%	23%	28%
Average Effectiveness	14%	28%	24.5%	29.5%

In addition, Figure 13c,d, together with Table 4, demonstrate that -DSK had different impacts on the temperature uniformity of the heat treatment in Config-2. It is observed that the usage of double-size skids first resulted in changes in the sorting of loads with respect to the maximum identified temperature non-uniformities. In the case of -DSK stacking, the lower block experienced higher temperature non-uniformities than the other blocks. This is in contrast with what was identified for Config-2-S0 (see Figure 11), where the middle block had the maximum non-uniformities, and Config-2-S5 and S-17, for which both the middle and lower blocks had a similar temperature non-uniformity (refer to Figure 12). This can be related to the diameter ratio of the spacer and skids with respect to the blocks. In Config-2, the ratio of skid diameter to the block thickness is higher than those of Config-1, where the large-size blocks are loaded. In Config-2, the lower block, which is in simultaneous contact with spacers and double-size skids, tolerated more severe temperature non-uniformities. In other words, although the -DSK results in the reduced distance between the fans and therefore provides better temperature uniformity, the high amount of added mass to the setup negatively affects the temperature uniformity of the lower block. This is because of the fact that the double-size skids in Config-2 act like an extra loading, which in turn

resulted in the stacking non-uniformity phenomenon. From Figure 13c,d, it can be seen that although the lower block experienced lower values of temperature non-uniformities in the peak area (by about 10%), higher temperature non-uniformities (16%) were observed later on toward the end of the process, resulting in a total of a 3% increase in temperature non-uniformities for this block. However, -DSK in Config-2 positively contributed to reducing the temperature non-uniformities for the middle and upper blocks. Therefore, although -DSK could contribute to the reduction of temperature non-uniformities of the stacked blocks in both configurations, its employment should always be in parallel with the consideration of the skid diameter to block diameter for the lower block, which is in direct contact with the skids. In other words, -DSK can be effectively used for heat treatment when the larger block is loaded as the lower block in the configuration.

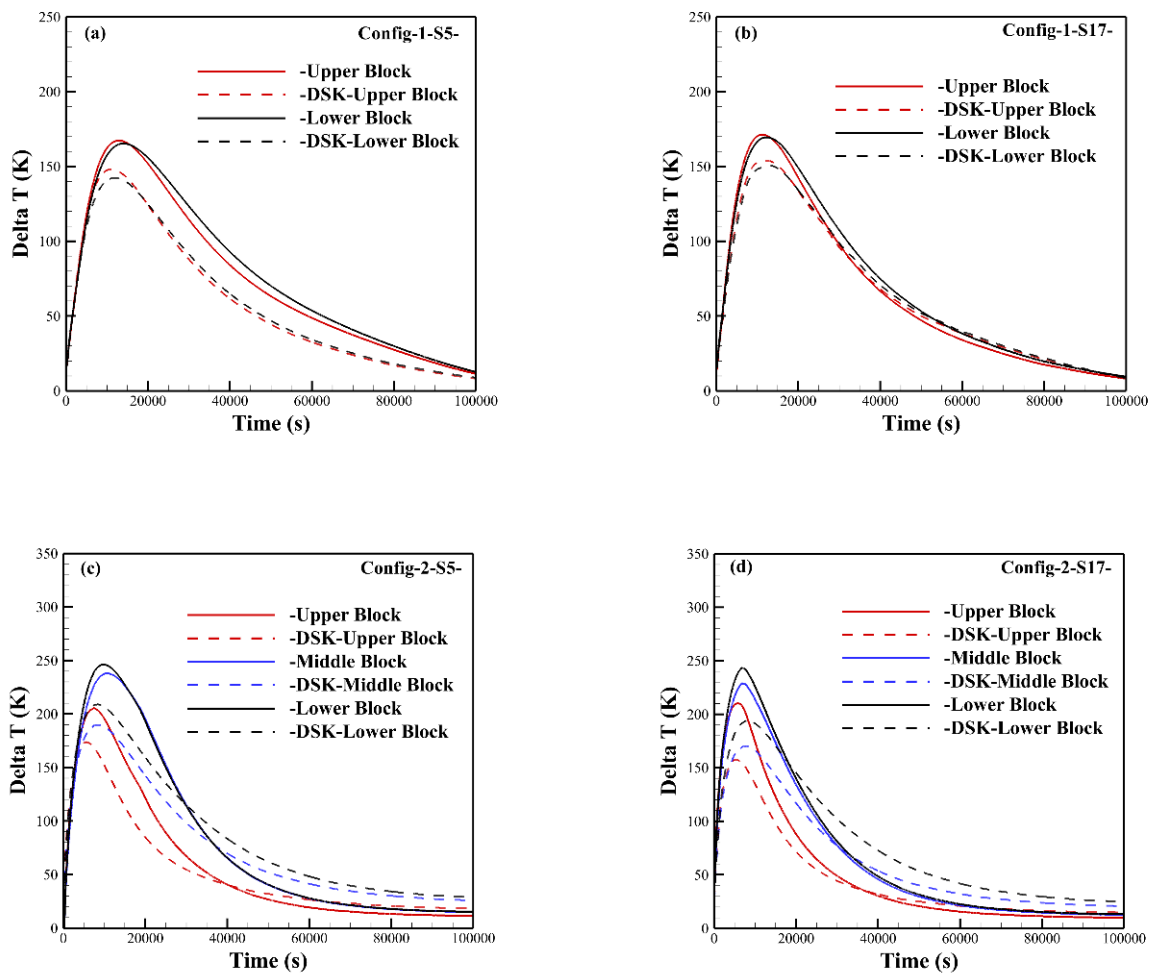


Figure 13. Double-size skids effect on temperature non-uniformities of products in (a) Config-1-S5, (b) Config-1-S17, (c) Config-2-S5, and (d) Config-2-S17.

Table 4. Effect of the double-size skid on temperature non-uniformity reduction of blocks in Config-2 relative to Config-2-S0.

Products	-S5	-S5-DSK	-S17	-S17-DSK
Lower Block	21%	18%	32%	28%
Middle Block	29%	35%	40%	45%
Upper Block	19%	28%	30%	37%
Average Effectiveness	23%	27%	34%	36.6%

7. Conclusions

A numerical analysis of the effect of the stacking pattern on the temperature uniformity of the high-strength steel parts during the heat treatment process within an industrial electrical furnace was performed. The 3D CFD model of the furnace, validated by real-scale experimental measurements, was employed to examine the effects of different spacers and skid sizes on the temperature uniformity of the products. Both convection and radiation heat transfer modes in a turbulent flow field of the heating chamber were taken into consideration. Two different setups of stacked forgings with different large-scale block sizes were used to increase the applicability of the present findings to the real practice of the heat treatment process in industrial sections. It was shown that using spacers of different sizes could affect temperature distribution at different stages. The optimum spacers-skids combination was determined for each configuration. The main conclusions of the investigation are summarized as follows:

1. The transient CFD model with MRF computation, covering practical details of the furnace, can be a reliable representative of the furnace under investigation. It is shown that the 3D CFD model predicted the transient temperature of the large-size blocks by a maximum average of 6.62% deviation during the heat treatment process.
2. It was shown that maximum temperature distribution non-uniformities of up to 200 K and 373 K could exist in the case of two rows and three rows of blocks stacked, respectively.
3. The effective usage of the spacers could significantly reduce the temperature distribution non-uniformities of the blocks by up to an average of 34% for the optimum spacer size.
4. The -S17 spacer size was identified as the optimum spacer size for both the large-size blocks and blocks stacking in this setup of materials.
5. The double-size skid could be effectively used for the heat treatment process, particularly when it comes to the stacking of large size blocks. Using this approach could increase the average effectiveness of temperature uniformity for large products by a maximum of 14%.
6. An adverse influence of the double-size skid was found for the heat treatment of the low thickness blocks.
7. The present CFD model and experimental data are applicable to the optimization of a furnace design and the operational conditions of industrial heat treatment furnaces.

Author Contributions: S.M.: conceptualization, methodology, software, validation, formal analysis, investigation, resources, data curation, writing—original draft preparation, writing—review and editing, visualization. N.B.A.: conceptualization, methodology, software, validation, formal analysis, investigation, data curation, writing—original draft preparation, writing—review and editing, visualization. F.B.-T.: supervision, methodology, formal analysis, writing—review and editing. J.-B.M.: conceptualization, investigation, supervision, resources, formal analysis. A.L.: investigation, resources, formal analysis, writing—review and editing. M.J.: conceptualization, methodology, supervision, formal analysis, writing—review and editing. All authors have read and agreed to the published version of the manuscript.

Funding: This work was funded by the Mitacs in the framework of [IT27097, IT03151] Grants.

Data Availability Statement: Not applicable.

Acknowledgments: The authors would like to extend their gratitude to Finkl Steel, especially its research and development and heat treatment departments, for providing the large blocks as well as the instrumentation and measurements used in these studies.

Conflicts of Interest: The authors declare no conflict of interest.

References

1. Kluczek, A.; Olszewski, P. Energy audits in industrial processes. *J. Clean. Prod.* **2017**, *142*, 3437–3453. [CrossRef]
2. Palacio-Caro, I.D.; Alvarado-Torres, P.N.; Cardona-Sepúlveda, L.F. Numerical Simulation of the Flow and Heat Transfer in an Electric Steel Tempering Furnace. *Energies* **2020**, *13*, 3655. [CrossRef]
3. Chan, D.Y.-L.; Yang, K.-H.; Lee, J.-D.; Hong, G.-B. The case study of furnace use and energy conservation in iron and steel industry. *Energy* **2010**, *35*, 1665–1670. [CrossRef]
4. Totten, G.E. *Steel Heat Treatment: Metallurgy and Technologies*; CRC Press: Boca Raton, FL, USA, 2006.
5. Kang, J.; Rong, Y. Modeling and simulation of load heating in heat treatment furnaces. *J. Mater. Process. Technol.* **2006**, *174*, 109–114. [CrossRef]
6. Askeland, D.R.; Wright, W.J. *Science and Engineering of Materials*; Nelson Education: Toronto, ON, Canada, 2015.
7. Gao, M.; Reid, C.N.; Jahedi, M.; Li, Y. Estimating equilibration times and heating/cooling rates in heat treatment of workpieces with arbitrary geometry. *J. Mater. Eng. Perform.* **2000**, *9*, 62–71. [CrossRef]
8. Gur, C.H.; Pan, J. *Handbook of Thermal Process Modeling Steels*; CRC Press: Boca Raton, FL, USA, 2008.
9. Bohlooli Arkhazloo, N.; Bazdidi-Tehrani, F.; Morin, J.-B.; Jahazi, M. Optimization of furnace residence time and loading pattern during heat treatment of large size forgings. *Int. J. Adv. Manuf. Technol.* **2021**, *113*, 2447–2460. [CrossRef]
10. U.S. Energy Information Administration, Manufacturing Energy Consumption Survey (MECS). Steel Industry Analysis Brief. Available online: <https://www.eia.gov/consumption/manufacturing/briefs/steel/> (accessed on 12 June 2022).
11. Arkhazloo, N.B.; Bouissa, Y.; Bazdidi-Tehrani, F.; Jadidi, M.; Morin, J.-B.; Jahazi, M. Experimental and unsteady CFD analyses of the heating process of large size forgings in a gas-fired furnace. *Case Stud. Therm. Eng.* **2019**, *14*, 100428. [CrossRef]
12. Bohlooli Arkhazloo, N. *Optimization of Furnace Residence Time and Ingots Positioning during the Heat Treatment Process of Large Size Forged Ingots*; École de Technologie Supérieure: Montréal, QC, Canada, 2020.
13. Zhang, S.; Wen, L.; Bai, C.; Chen, D.; Long, Z. Analyses on 3-D gas flow and heat transfer in ladle furnace lid. *Appl. Math. Model.* **2009**, *33*, 2646–2662. [CrossRef]
14. Chattopadhyay, K.; Isac, M.; Guthrie, R. Applications of Computational Fluid Dynamics (CFD) in iron-and steelmaking: Part 1. *Ironmak. Steelmak.* **2010**, *37*, 554–561. [CrossRef]
15. Wang, Z.J.; Shang, X.F. Flow and Heat-Transfer Simulation Based on CFD and Experimental Study during High-Pressure Gas Quenching. In *Applied Mechanics and Materials*; Trans Tech Publications: Stafa-Zurich, Switzerland, 2010.
16. Arkhazloo, N.B.; Bazdidi-Tehrani, F.; Jadidi, M.; Morin, J.-B.; Jahazi, M. Determination of temperature distribution during heat treatment of forgings: Simulation and experiment. *Heat Transf. Eng.* **2022**, *43*, 1041–1064. [CrossRef]
17. Harish, J.; Dutta, P. Heat transfer analysis of pusher type reheat furnace. *Ironmak. Steelmak.* **2005**, *32*, 151–158. [CrossRef]
18. Mayr, B.; Prieler, R.; Demuth, M.; Moderer, L.; Hochenauer, C. CFD analysis of a pusher type reheating furnace and the billet heating characteristic. *Appl. Therm. Eng.* **2017**, *115*, 986–994. [CrossRef]
19. Tang, G.; Wu, B.; Bai, D.; Wang, Y.; Bodnar, R.; Zhou, C.Q. Modeling of the slab heating process in a walking beam reheating furnace for process optimization. *Int. J. Heat Mass Transf.* **2017**, *113*, 1142–1151. [CrossRef]
20. Liu, Y.; Li, J.; Misra, R.; Wang, Z.; Wang, G. A numerical analysis of slab heating characteristics in a rolling type reheating furnace with pulse combustion. *Appl. Therm. Eng.* **2016**, *107*, 1304–1312. [CrossRef]
21. Yang, Y.; De Jong, R.A.; Reuter, M.A. CFD prediction for the performance of a heat treatment furnace. *Prog. Comput. Fluid Dyn. Int. J.* **2007**, *7*, 209–218. [CrossRef]
22. Prieler, R.; Mayr, B.; Demuth, M.; Spoljaric, D.; Hochenauer, C. Application of the steady flamelet model on a lab-scale and an industrial furnace for different oxygen concentrations. *Energy* **2015**, *91*, 451–464. [CrossRef]
23. Govardhan, J.; Rao, G.; Narasaiah, J. Experimental investigations and CFD study of temperature distribution during oscillating combustion in a crucible furnace. *Int. J. Energy Environ.* **2011**, *2*, 783–796.
24. Singh, V.K.; Talukdar, P.; Coelho, P.J. Performance evaluation of two heat transfer models of a walking beam type reheat furnace. *Heat Transf. Eng.* **2015**, *36*, 91–101. [CrossRef]
25. Galletti, C.; Coraggio, G.; Tognotti, L. Numerical investigation of oxy-natural-gas combustion in a semi-industrial furnace: Validation of CFD sub-models. *Fuel* **2013**, *109*, 445–460. [CrossRef]
26. Filipponi, M.; Rossi, F.; Presciutti, A.; De Ciantis, S.; Castellani, B.; Carpinelli, A. Thermal analysis of an industrial furnace. *Energies* **2016**, *9*, 833. [CrossRef]
27. Díaz-Ovalle, C.O.; Martínez-Zamora, R.; González-Alatorre, G.; Rosales-Marines, L.; Lesso-Arroyo, R. An approach to reduce the pre-heating time in a convection oven via CFD simulation. *Food Bioprod. Process.* **2017**, *102*, 98–106. [CrossRef]
28. Tan, S.A.; Yu, K.H.; Abdullah, M.Z. Heat transfer analysis on wafer annealing process in semiconductor multi-wafer furnace using CFD simulation. *J. Mech. Sci. Technol.* **2022**, *36*, 3143–3151. [CrossRef]
29. Amanlou, Y.; Khoshtaghaza, M.H. Applications of CFD for Optimization of Cabinet Dryers. In *Computational Fluid Dynamics in Food Processing*; CRC Press: Boca Raton, FL, USA, 2018; pp. 415–436.
30. Ismail, O.S.; Awonusi, A.A.; Akinoso, R. Isothermal Air Flow Investigation in Industrial Baking Oven of Different Impeller Locations using Computational Fluid Dynamics (CFD) Approach. *J. Eng. Sci.* **2021**, *17*, 73–91. [CrossRef]
31. Fu, Z.; Yu, X.; Shang, H.; Wang, Z.; Zhang, Z. A new modelling method for superalloy heating in resistance furnace using FLUENT. *Int. J. Heat Mass Transf.* **2019**, *128*, 679–687. [CrossRef]

32. Macchion, O.; Zahrai, S.; Bouwman, J. Heat transfer from typical loads within gas quenching furnace. *J. Mater. Process. Technol.* **2006**, *172*, 356–362. [[CrossRef](#)]
33. Korad, T.; Ponboon, M.; Chumchery, N.; Pearce, J.T.H. Overview of Flow Analysis Simulation in Improving Heat Treatment Conditions. *Chiang Mai J. Sci.* **2013**, *40*, 898–908.
34. Finkl Steel Inc. Saint-Joseph-de-Sorel, QC, Canada. Available online: <http://www.sorelforge.com/> (accessed on 10 February 2022).
35. OmegaEngineering. Thermocouple Types. 2022. Available online: <https://www.omega.ca/en/resources/thermocouple-types> (accessed on 12 June 2022).
36. ANSYS. *ANSYS Fluent Theory Guide*; ANSYS, Inc.: Canonsburg, PA, USA, 2013.
37. Versteeg, H.K.; Malalasekera, W. *An Introduction to Computational Fluid Dynamics: The Finite Volume Method*; Pearson Education: London, UK, 2007.
38. Hadała, B.; Malinowski, Z.; Rywotycki, M. Energy losses from the furnace chamber walls during heating and heat treatment of heavy forgings. *Energy* **2017**, *139*, 298–314. [[CrossRef](#)]
39. Saunders, N.; Guo, U.K.; Li, X.; Miodownik, A.P.; Schillé, J.P. Using *JMatPro* to model materials properties and behavior. *JOM* **2003**, *55*, 60–65. [[CrossRef](#)]

Disclaimer/Publisher’s Note: The statements, opinions and data contained in all publications are solely those of the individual author(s) and contributor(s) and not of MDPI and/or the editor(s). MDPI and/or the editor(s) disclaim responsibility for any injury to people or property resulting from any ideas, methods, instructions or products referred to in the content.